

Target-directed dynamic combinatorial chemistry affords inhibitors of Nsp10 as potential antivirals against SARS-CoV-2

Ravindra P. Jumde ^{1#}, Gwenaëlle Jézéquel ^{1#}, Margarida Saramago ², Nicolas Frank ^{1,3}, Sebastian Adam ¹, Marta V. Cunha ², Chantal Bader ¹, Antonia P. Gunesch ⁴, Natalie M. Köhler ⁴, Sandra Johannsen ^{1,3}, Thomas Pietschmann ^{4,5}, Rute G. Matos ², Rolf Müller ^{1,3,6}, Cecília M. Arraiano ², Anna K.H. Hirsch ^{1,3,6,*}

¹ Helmholtz Institute for Pharmaceutical Research Saarland (HIPS) – Helmholtz Centre for Infection Research (HZI), Campus E 8.1, 66123 Saarbrücken, Germany

² Instituto de Tecnologia Química e Biológica António Xavier, Universidade Nova de Lisboa, Avenida da República, 2780-157 Oeiras, Portugal

³ Department of Pharmacy, Saarland University, Campus E 8.1, 66123 Saarbrücken, Germany

⁴ Institute for Experimental Virology, Twincore - Centre for Experimental and Clinical Infection Research; Feodor-Lynen-Str. 7, 30625 Hannover, Germany.

⁵ Cluster of Excellence RESIST (EXC 2155), Hannover Medical School; 30625 Hannover, Germany

⁶ Helmholtz International Lab for Anti-infectives, Campus E 8.1, 66123 Saarbrücken, Germany

These authors contributed equally to this work.

*Corresponding author: A.K.H. Hirsch anna.hirsch@helmholtz-hips.de

Abstract: The development of antiviral drugs against the Severe Acute Respiratory Syndrome coronavirus 2 (SARS-CoV-2) responsible for the recent worldwide Covid-19 pandemic is important, as treatment options are still very limited and vaccination largely does not prevent infection. Two underexplored potential targets of this virus are the 3'-to-5' exoribonuclease (ExoN) and the 2'-O-methyltransferase (2'-O-Mtase), which are essential for the viability of the virus. The non-structural protein Nsp14 displays the first enzymatic activity, and Nsp16 the latter, especially while in complex with their co-factor protein Nsp10. Herein, we report the use of target-directed dynamic combinatorial chemistry to find binders of Nsp10, in the aim of preventing the formation of the Nsp10-Nsp14 and Nsp10-Nsp16 protein-protein interaction (PPI). We synthesised the hits, and tested them for their affinity Nsp10 affinity, their inhibition of ExoN and 2'-O-methyltransferase activities, as well as their anti-viral potential in a hCoV-229E and SARS-CoV-2 whole-cell setting. We report a novel class of inhibitors of ExoN and/or 2'-O-methyltransferase activities that present an anti-viral activity against coronaviruses.

Introduction:

The end of the year 2019 saw the emergence of the Severe Acute Respiratory Syndrome coronavirus 2 (SARS-CoV-2), a new coronavirus that led to the worldwide Covid-19 pandemic.^{1,2} The fast development of vaccines lowered the impact of the outbreak, especially on the hospitals that were saturated with patients. However, there is still a need for SARS-CoV-2 therapeutics due to the persistent number of infections caused by the emergence of virus variants, incomplete vaccination and the difficulty in developing specific drugs including such from drug repurposing.³ SARS-CoV-2 is a positive-sense single-stranded RNA virus, and codes for four structural proteins, and two polyproteins.⁴ After cleavage by the main protease (M^{pro}), those polyproteins yield 16 nonstructural proteins (Nsp) that have RNA-processing and RNA-modifying functions essential for the viral replication.⁵

Among these Nsp, Nsp14 is a bifunctional non-structural protein displaying two essential activities: an N-terminal 3'-to-5' exoribonuclease activity (ExoN) and a C-terminal N7-methyltransferase activity (N7-MTase), located on two distinct domains.⁶ Interestingly, the

ExoN activity is specific and crucial to coronaviruses, as it ensures reliability of the replication process.⁷ SARS-CoV-2 ExoN knockout mutants are not viable, contrary to the SARS-CoV-1 and Mouse Hepatitis Virus (MHV) knockout mutants that show a high mutation frequency, but no lethality.^{8–10} Inhibiting this enzymatic activity therefore appears to be a relevant strategy to develop new specific antivirals against SARS-CoV-2. Strikingly, the ExoN activity of Nsp14 is strongly stimulated in a dose-dependent manner by the formation of a stable complex with Nsp10, which then acts as a cofactor.¹¹ While Nsp14 alone still displays an exoribonuclease activity, it is orders of magnitude lower than when in complex with Nsp10.¹²

It is interesting to note that Nsp10 acts as a cofactor for Nsp16 as well, to display a 2'-O-methyltransferase (2'-O-MTase) activity.¹³ The 2'-O-MTase forms part of the replication-transcription complex, and its binding partner, Nsp10, regulates its activity. It plays an essential role in host immune evasion by mimicking its human homolog, Cap-specific mRNA(nucleoside-2'-O)-methyltransferase (CMT1), to perform a crucial step in capping transcribed mRNA.^{13,14} The 2'-O-Mtase knockout mutants show attenuation of viral replication and infectivity of coronaviruses in the host.^{15,16}

Nsp10 is therefore an essential protein for viral replication, though it does not have an activity *per se*, but is a crucial activation factor for both Nsp14 and Nsp16.¹⁷ Finding disturbers of the Nsp10-Nsp14 and/or Nsp10-Nsp16 protein-protein interactions (PPI) targets both ExoN and MTase activities and therefore represents a promising strategy to develop new antivirals against SARS-CoV-2. Moreover, crystal structures of Nsp10 have been unravelled, either alone or in complex with Nsp14 or Nsp16.^{18–20}

Some approved drugs have been repurposed for the treatment of Covid-19, with limited success, except for the combination of nirmatrelvir/ritonavir (Paxlovid) for which the FDA granted an emergency use authorisation.^{21,22} Remdesivir is the only fully FDA-approved therapy for COVID-19, and so far it is still the only one. It is an antiviral drug that belongs to the type of nucleoside analogue inhibitors (NAs) targeting the RNA-dependent RNA-polymerase (Nsp12 in CoVs).²³ However, the use of NAs in coronavirus is challenging due to the presence of the Nsp14 ExoN proofreading activity. Nsp14 is known to reduce the inhibitory effect of drugs that function through premature termination of viral genome replication.^{7,10,24–26} Taking this into account, Nsp14 is particularly important as a drug target.³ Some efforts to find inhibitors of ExoN activity in SARS-CoV-2, either by *in silico* screening, high-throughput biochemical screening or fragment approaches led to the discovery of interesting compounds^{27–30}. However, the mode of action of some of the identified hits is not clear, and all will need further optimisation in terms of activity and selectivity. Similarly, for the 2'-O-Mtase target, most of the reported inhibitors are adenosyl analogues, which suffer from selectivity issues for viral over human MTases causing (cyto)toxic effects. Despite recent medicinal-chemistry efforts, only very few non-adenosyl inhibitors are reported with questionable activity (only virtual docking scores, or poor selectivity).^{31–33}

To target the ExoN and MTase activities, we set out to find new hits that would inhibit the PPIs of these proteins with Nsp10. Due to the lack of potent inhibitor/s of these enzymes of SARS-CoV-2, there is a need to use hit-identification strategies other than traditional medicinal-chemistry approaches. One of the hit-identification strategies that does not require the knowledge of inhibitors is target-directed dynamic combinatorial chemistry (tdDCC), which emerged as an efficient hit-identification strategy in the past two decades.^{34,35} In protein-templated DCC in particular, a dynamic combinatorial library (DCL) is incubated with the target protein, which will modify the equilibrium by selecting and amplifying its binders. This powerful tool already allowed the fast discovery and optimisation of new inhibitors for various targets, including PPI targets.^{36–39}

Inhibition of ExoN and MTase activities, by blocking their interactions with Nsp10, appeared to be a good strategy to develop antiviral compounds against SARS-CoV-2. Additionally, the scarcity of inhibitors of these enzymes makes tdDCC a particularly attractive hit-identification approach for the discovery of new inhibitors.

Results and discussion:

Nsp10 presented itself as suitable target protein for our tdDCC approaches for several reasons. Firstly, it is stable and soluble at room temperature, confirmed by thermal shift assays (for details see SI). Secondly, the protein is small (140 amino acids) with a well-defined PPI domain interacting with Nsp14 and another one with Nsp16.¹¹ As Nsp10 is a co-factor for both proteins, therefore directing our hit-finding strategy toward it could allow the discovery of inhibitors for either Nsp14 or Nsp16, or even of a dual inhibitor compound.

Set-up of the tdDCC:

To introduce a broad range of structural diversity, we conducted two rounds of tdDCC with different DCLs. They both contain three aldehydes and seven (DCL-1) or eight (DCL-2) hydrazides, respectively (Figure 1). We chose a wide range of aldehyde and hydrazide building blocks in both DCLs, including different aromatic and heterocyclic rings with different functional groups and linkers to cover a wide chemical space with good structural diversity. We included aromatic rings with electron-withdrawing (nitro, dichloro, fluoro and trifluoromethyl) and donating (hydroxyl, amine, and methyl) groups, as well as polar (sulfonyls, dioxane, nitro, and hydroxyl) groups to study the effect on the biological activity of the potential hits under physiological conditions. We also chose different sizes of flexible linkers to explore the length of the pocket (zero to four carbons between the hydrazide and adjacent moieties).

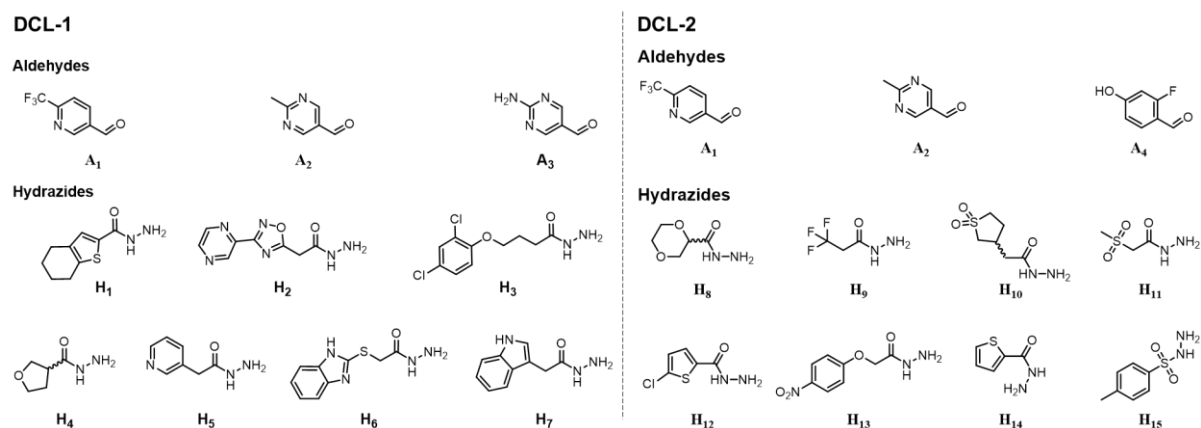


Figure 1 - Dynamic Combinatorial Libraries (DCLs) used for target-directed Dynamic Combinatorial Chemistry-1 (tdDCC-1) and tdDCC-2. For both tdDCCs, the experiment was run in phosphate buffer (pH 7.04) and 5% DMSO with the aldehydes (100 μ M each, in DMSO), hydrazides (300 μ M each, in DMSO), aniline (10 mM in DMSO) and the Nsp10 protein (50 μ M in phosphate buffer).

We performed both tdDCCs in the same way. Reaction of the building blocks in phosphate buffer with an excess of aniline and 5% DMSO led to the DCLs, one without the protein (blank) and two duplicates in presence of Nsp10 (namely, protein-templated I and protein-templated II). The composition of blank DCL was analysed by UPLC-MS to study the equilibrium of acylhydrazone formation. The periodic samples from blank and protein-templated DCLs were treated with NaOH to freeze the acylhydrazone formation and with acetonitrile to denature the protein. After reaching the equilibrium, comparison of an adaptive DCC experiment in presence

of Nsp10 protein with the corresponding blank DCL enabled identification of the amplified acylhydrazones.

tdDCC-1

The first step in a tdDCC experiment is to determine the time required to reach equilibrium. For this purpose, we identified all the products in the mixture (21 acylhydrazones) by their respective mass from the UPLC-MS runs, and the evolution of their relative peak area (RPA) was plotted as a function of time. The system is considered stabilised when there are no considerable changes in the relative peak areas of the various acylhydrazones.³⁷ For tdDCC-1, this equilibrium was reached after 26 hours (Figure 2a). We then compared the RPAs of the two protein-templated duplicates with the blank to determine the amplification of the respective compounds (Figure 2b and 2c). We identified four significantly amplified hits (**1–4**) with a RPA change over 0.5%, two slightly amplified with a RPA change between 0 and 0.5% (**5, 6**) (Figure 2d) and decided to consider two random depleted hits (**7, 8**) as a control (Figure 4a). Analysing the structures of amplified hits revealed that trifluoromethylpyridine (**A1**), methyl- (**A2**) and amino-pyrimidines (**A3**) from the aldehyde part were all found among the hits. Out of them, the 2-aminopyrimidine moiety is present in the top two amplified hits (**1** and **2**) followed by 2-methylpyrimidine (**3** and **5**) and 2-trifluoromethylpyridine (**4** and **6**). Moreover, on the hydrazide part, the pyridine containing hydrazide **H5** seems to be more favoured as it appears twice in hits **1** and **5**. The hydrazide **H1**, **H2**, **H4**, and **H7** are present in hits **4**, **6**, **2**, and **3**, respectively. The two hydrazides **H3** and **H6** did not appear in any of the amplified hits. Regarding electron density, both electron-rich (**H4**) and electron-poor (**H5**) hydrazides are present in the hits (compound **2** and compounds **1** and **5** respectively).

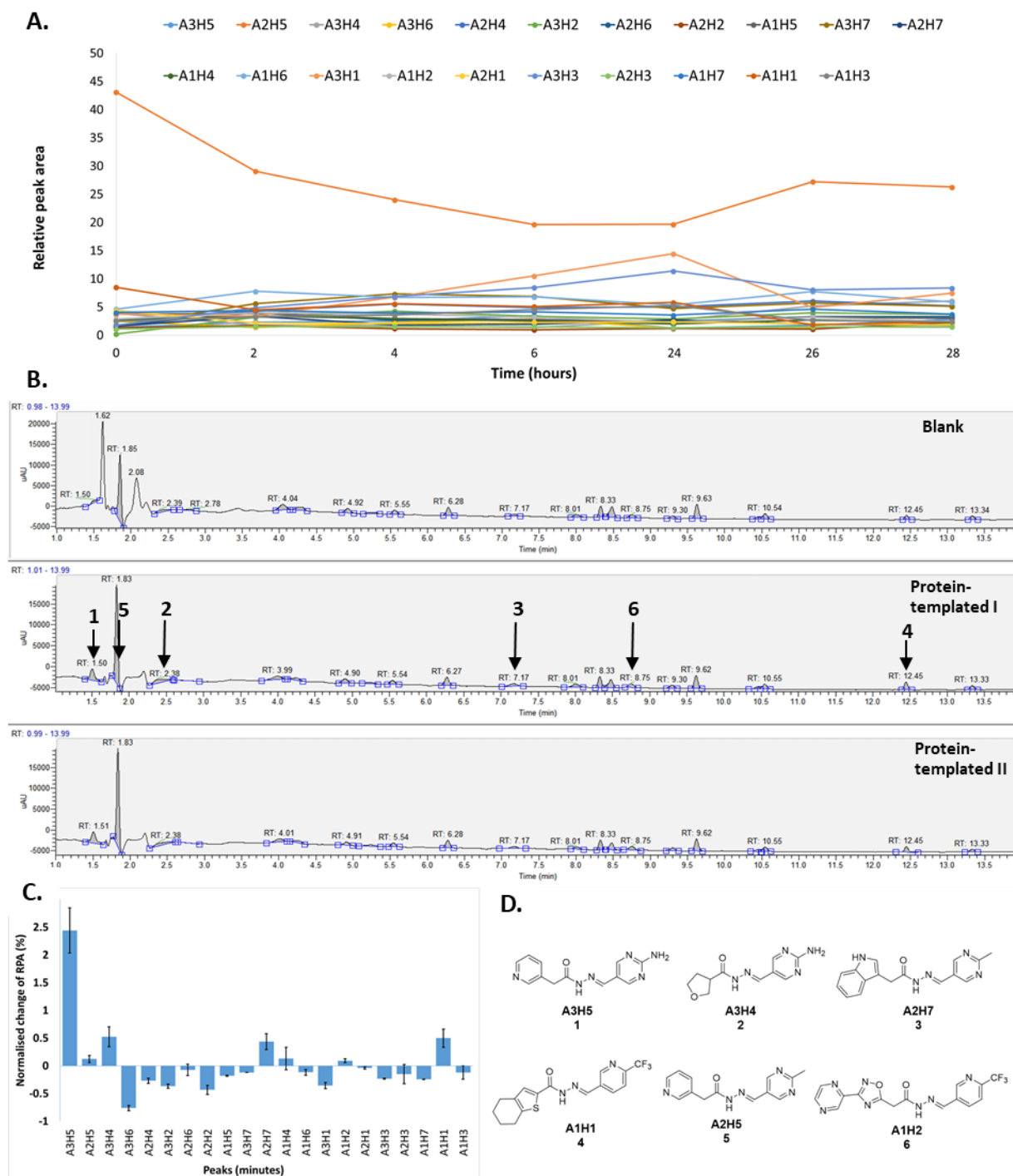


Figure 2 - tdDCC-1. A - Evaluation of the relative peak areas of the different acylhydrazone concentrations over time and determination of the equilibrium. B - Comparison between the blank and the protein-templated experiments' relative peak areas. C - Normalised relative amplification of the products in the protein-templated DCC experiments compared to the blank. D - Structure of the significantly and slightly amplified hits.

tdDCC-2

Similarly to tdDCC-1, the equilibrium for tdDCC-2 was determined after the identification of the products in the mixture. We did not include the compound **A1H9** in the analysis, as even though we could detect it by MS, its formation was probably very low and undetectable by UV absorption. As for compounds **A1H15** and **A2H15** were not detected by LCMS, probably due

to the decomposition during the basic treatment and/or during the ionization. In contrast to the acylhydrazones, the proton adjacent to the nitrogen in the *p*-toluenesulfonylhydrazones is susceptible for the base attack, which can lead to the formation of an unstable diazo compounds.⁴⁰ However, we could detect by mass the trace amount of compound **A4H15** that also contains a *p*-toluenesulfonyl hydrazine moiety, but under the same peak as compound **A1H14**. The latter situation, where two products had the same retention time, appeared three times in total. We then treated the two mixed compounds as one product for the equilibrium and amplification analysis (**A4H15 + A1H14**, **A4H8 + A2H14** and **A4H14 + A4H9**) and consider the positively amplified ones as potential hits. This points to the problems associated with large-scale tdDCC, where there is a risk of different products eluting at the same retention time.

TdDCC-2 reached equilibrium after eight hours (Figure 3a), enabling comparison of the RPAs between the blank and the protein-templated experiments (Figure 3b) and the calculation of the amplification (Figure 3c). This comparison revealed that the compound **9** was significantly amplified, and compound **10** was slightly amplified in the tdDCC-2 experiment (Figure 3d). The peak corresponding to the two compounds **11/12** was also slightly amplified, therefore we chose to consider both as potential hits. Finally, compounds **13/14** are slightly depleted, we therefore could not draw any conclusion from the amplification analysis. As for tdDCC-1, we chose two compounds (**15** and **16**) among the depleted amplifications for control (Figure 4a). Along with the depleted compounds **15** and **16** as a negative control, we also chose to synthesise compounds **13** and **14**, which eluted under the same peak and are slightly depleted. Similarly to tdDCC-1, each of the three different aldehydes (**A1**, **A2**, **A4**) is present twice among the hit compounds. Regarding the hydrazide part, the thiophene or chlorothiophene moieties are present in three of the six hits (**9**, **11**, **13**), thus might have been playing a significant role in the amplification. Both polar (**H8**) and apolar (**H12**, **H14**) groups containing hydrazides are amplified (compounds **8**, **10** and **14**, **11** and **13** respectively). Once again, both electron-rich (**H12**, **H14**) and electron-poor (**H15**) hydrazides gave amplified compounds (compounds **9**, **11**, **13** and **12** respectively).

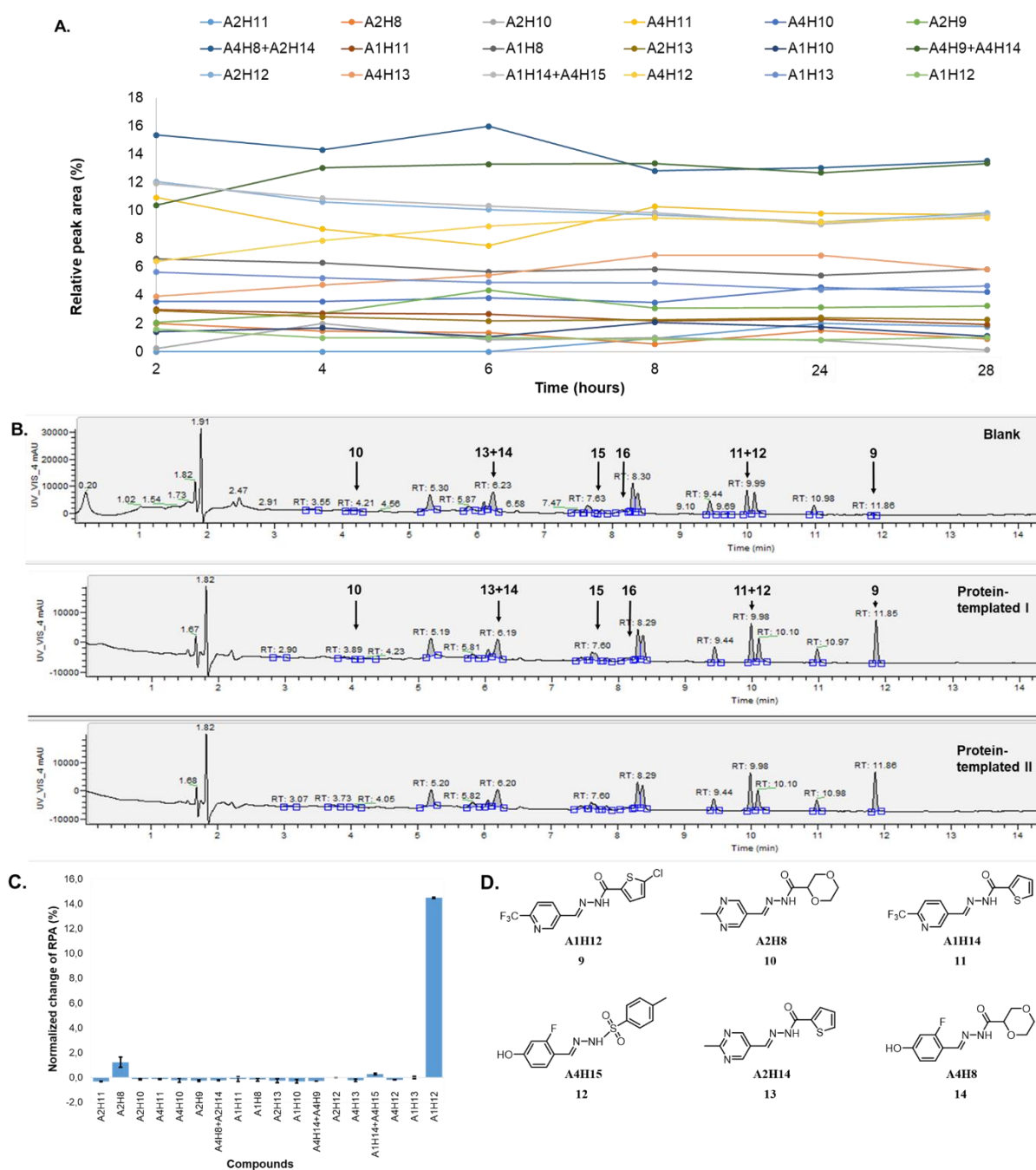


Figure 3 - tdDCC-2. A - Evaluation of the relative peak areas of the different acylhydrazone concentrations over time and determination of the equilibrium. B – Comparison between the blank and the protein-templated experiments' relative peak areas. C - Normalised relative amplification of the products in the protein-templated DCC experiments compared to the blank. D - Structure of the significantly and slightly amplified hits.

To confirm the activity of our hits, we selected the significantly and slightly amplified hits (**1–6** and **9–12** Figure 2d and 3d), as well as two random controls among the depleted compounds (**7, 8, 15, and 16**, Figure 4a) for each DCL. We also synthesised compounds **13–14** (Figure 3d) to check for their actual activity. We accessed all the selected acylhydrazone hits, as well as the control compounds in one step, by reacting aldehyde and corresponding hydrazide in methanol at 65 °C, with moderate to excellent yield (Figure 4b).³⁶

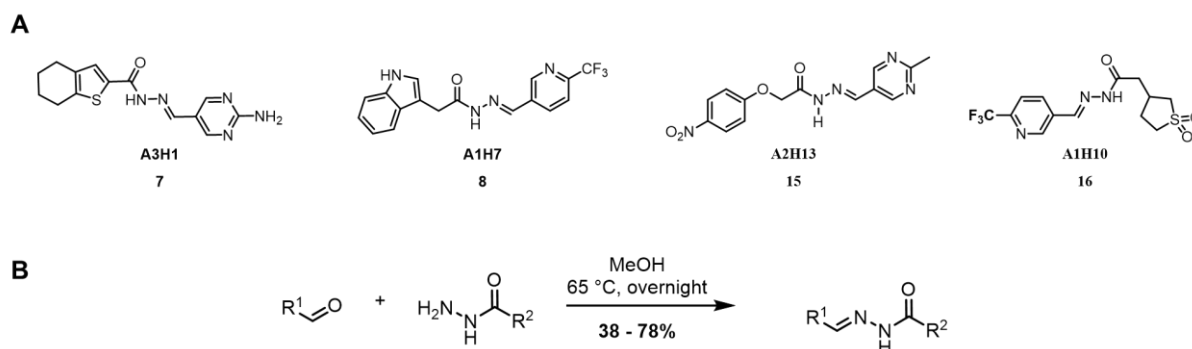


Figure 4 – A - Controls chosen among depleted compounds for tdDCC-1 (**7** and **8**) and tdDCC-2 (**15** and **16**). B – General scheme of the synthesis of the acylhydrazones. Reaction conditions: the hydrazide (1.0 equiv.) and the aldehyde (1.0 equiv.) are suspended in MeOH and stirred overnight at 65 °C.

Binding affinity of tdDCC-1 & -2 hits

We evaluated all the synthesised compounds (**1–16**) for their binding affinity to Nsp10 by a native mass spectrometry (MS) analysis. Native mass spectrometry is a versatile method that enables the analysis of proteins and their non-covalently driven assemblies in their native or near-native state by spraying them from non-denaturing solvents.⁴¹ Thus, if the ligand binds to the protein, the mass of the complex is detected with an intensity proportional to the binding affinity. It is an easy, efficient and quick method that can be used to do high-throughput screening of potential inhibitors. Most of the synthesised compounds bind Nsp10 as the complex mass was detected by native MS, except for compounds **2**, **7** and **9**; compound **16** shows unspecific binding (Table 1). Nevertheless, even for the compounds that are binding, the intensity of complex protein-ligand peak was low compared to the intensity of the protein peak alone, indicating that the binding affinity is weak (Figure 5).

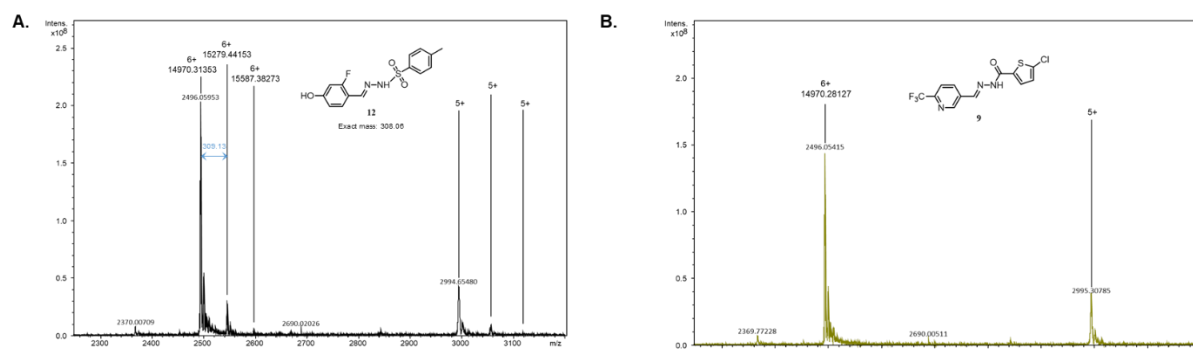


Figure 5 – Native MS spectra examples from some tdDCC hits. A – Analysis of low binding affinity compound **12** displays a complex mass peak with a low intensity compared to the protein mass peak. B – Analysis of non-binding compound **9** does not show a mass peak corresponding to the complex mass.

To better characterise the binding affinity of the compounds, we then proceeded to an orthogonal analysis by Surface Plasmon Resonance (SPR). Compounds **1–8** showed a double-digit micromolar affinity (15–170 μ M), compound **12** displayed a K_D of 200 μ M and the rest of the compounds did not show any significant binding to Nsp10 by SPR (Table 1). The 2-aminopyrimidine motif seems beneficial for the affinity of this class with Nsp10, as it is present in the two best binders **1** and **7**. Moreover, compounds **1** and **5** bear a pyridine moiety, and also display good K_D . However, the lower molecular weight hit compounds from tdDCC-2 (**9–11**, **13**, **14**) do not show any affinity. The only compound from the tdDCC-2 that shows a weak affinity is a high-molecular weight compound **12**. Therefore, it appears that the hydrazide part should bear at least one aromatic ring with a spacer to be able to bind with Nsp10 (with the

exception of compound **2**, that displays a good affinity albeit its smaller size). It appears that when the K_D is in the 15–100 μM , a weak intensity of the near-native MS signal is detected. However, above 100 μM , the correlation does not exist anymore, and we can witness false positive and negative. If near-native MS can be a first intention screening method for the binding affinity, the SPR is complementary and necessary to assess the actual affinity.

Table 1 – Binding affinity of the tdDCC hits with Nsp10 determined by native MS and SPR analysis^a

Compound d	Native MS	K_D on Nsp10 (μM)	Compound d	Native MS	K_D on Nsp10 (μM)
1	weak intensity	15 \pm 3	9	complex not detected	n.b.
2	complex not detected	160 \pm 40	10	weak intensity	n.b.
3	weak intensity	100 \pm 10	11	weak intensity	n.b.
4	weak intensity	90 \pm 10	12	weak intensity	200 \pm 60
5	weak intensity	80 \pm 10	13	weak intensity	n.b.
6	weak intensity	120 \pm 10	14	weak intensity	n.b.
7	complex not detected	170 \pm 20	15	weak intensity	n.b.
8	weak intensity	130 \pm 10	16	unspecific binding	n.b.

^a The affinity of the synthesised compounds for Nsp10 was measured by Surface Plasmon Resonance with a 24 μM concentration of Nsp10 in sodium acetate buffer.
n.b.: no binding

Effect of the synthesised compounds on the 3'-5' exoribonuclease enzymatic activity of SARS-CoV-2 Nsp14

As we designed compounds that can interact with the PPI site of the Nsp10/Nsp14 complex and eventually inhibit the ExoN activity of Nsp14, we tested their effect in the SARS-CoV-2 Nsp14 capacity to degrade RNA *in vitro*. For that, all the compounds were previously incubated with Nsp10 for a few minutes and then we allowed the reaction to proceed. The results have shown that the synthesised compound **9** significantly inhibits the ExoN activity of Nsp14 (Figure 6). Compounds **4**, **7** and **11** also decreased the capacity of Nsp14 enzyme to degrade the RNA substrate. Each compound was titrated to determine the respective IC *in vitro* (Figure 6). Compound **9** was the one that showed the lower IC₅₀ value, confirming its higher capability of inhibiting nsp14 ExoN activity. We have performed a similar experimental setup, but this time we have incubated the compound **9** with a pre-formed Nsp14/Nsp10 complex. Interestingly, this compound was able to disrupt the ExoN enzymatic activity even in these conditions (data not shown). Compounds **4**, **9** and **11** share the 2-(trifluoromethyl)pyridine motif, which therefore seems beneficial for the inhibition of ExoN activity. They also all bear a thiophene, either as a simple thiophene (**11**), a chlorothiophene (**9**) or in a tetrahydrobenzothiophene moiety (**4** and **7**). An electron-rich apolar motif on this side of the molecule therefore is highly beneficial for this activity.

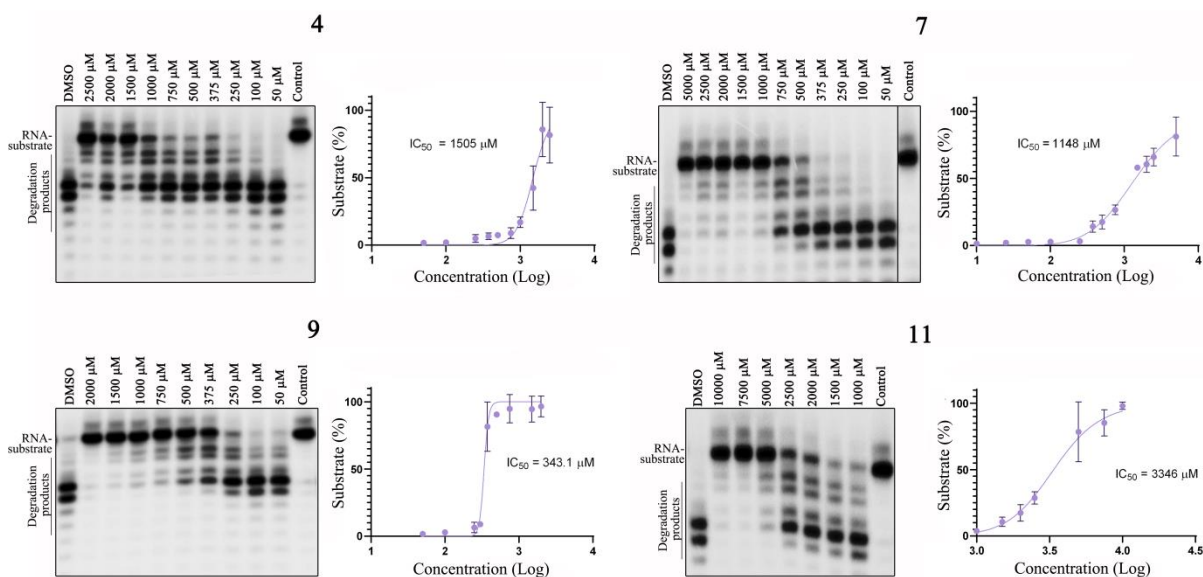


Figure 6 – Inhibition of the 3'-5' exoribonuclease activity of SARS-CoV-2 Nsp14 by compounds **4**, **7**, **9** and **11**. 500 nM of Nsp14 and 2000 nM of Nsp10 were incubated with 50 nM of RNA substrate in the presence of 50 to 10.000 μM of each compound. Reactions were analysed on 7 M urea / 20 % polyacrylamide gels. C, control reactions with no enzymes; DMSO, reactions performed in the absence of any compound but with DMSO. All the experiments were performed at least in triplicate. The amount of RNA substrate at the end of the reaction was quantified in the presence of different concentrations of each compound, and the IC_{50} was determined for each compound.

Influence of the synthesised compounds on the 2'-O-methyltransferase activity of SARS-CoV-2 Nsp16

Considering that we designed the tdDCC to find binders of Nsp10 which is also a co-factor for Nsp16, our compounds could potentially also interfere on the Nsp10/Nsp16 interaction. Moreover, as some residues involved in both interactions (Nsp10/Nsp14 and Nsp10/Nsp16) are the same, some of the compounds could have a dual inhibition.⁴² Considering this, we tested the effect of all compounds on the MTase activity of Nsp16/Nsp10. From the 16 compounds tested, we observed that compounds **11**, **13** and **14** were able to inhibit the MTase activity on a dose depending manner (Figure 7), with compound **13** presenting the lower IC_{50} value (429.7 μM). Interestingly compound **11** was able to inhibit both the ExoN and MTase activities of Nsp14/Nsp10 and Nsp16/Nsp10 complexes, although it was much more effective in inhibiting the Nsp16 MTase activity (Figures 6 and 7). These results show that compound **11** has a dual role and therefore it is a good candidate for further development as a dual inhibitor.

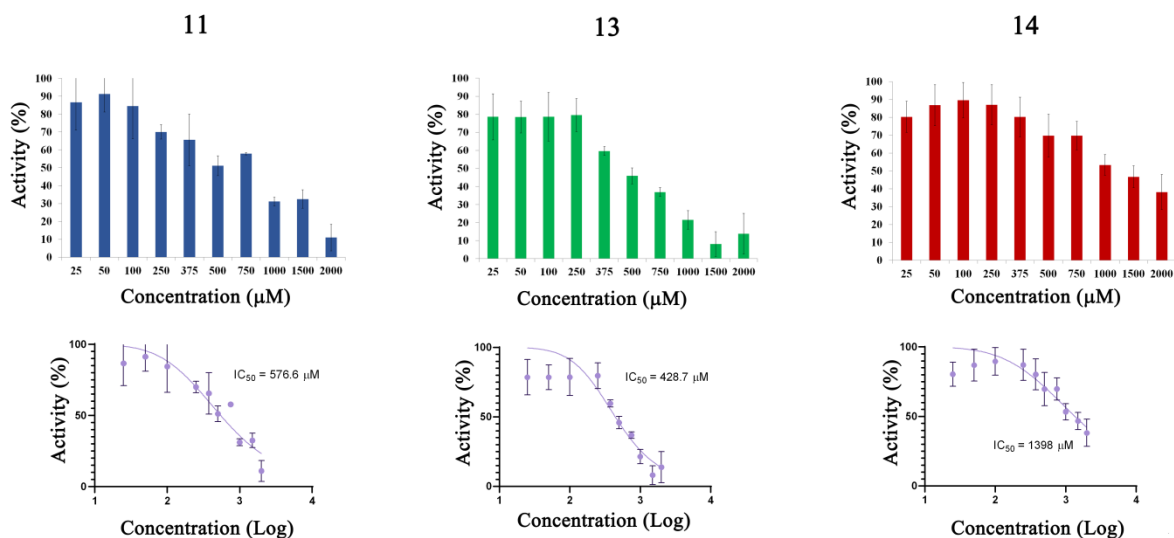
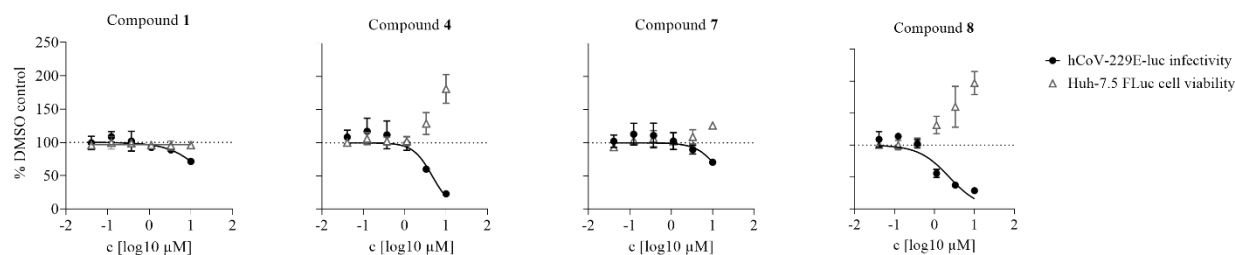


Figure 7 – Inhibition of the 2'-O-methyltransferase activity of SARS-CoV-2 Nsp16 by compounds **11**, **13** and **14**. 500 nM of Nsp16 and 2000 nM of Nsp10 were incubated with 50 nM of capped RNA substrate in the presence of 25 to 2000 μM of each compound. The formation of the reaction product SAH was determined by luminescence. Control reactions with no enzymes and with the enzymes in the presence of DMSO were performed to determine 0 and 100 % of activity. All the experiments were performed at least in triplicate. The IC₅₀ was determined for each compound.

Whole-cell antiviral activity against hCoV-229E

Finally, we wanted to evaluate the hits as potential antiviral agents against coronaviruses. We tested them against human coronavirus 229E (hCoV-229E) from alphacoronavirus family, which is one of the viruses responsible for the common cold.⁴³ SARS-CoV-2 (from a betacoronavirus family) and hCoV-229E share 67% of sequence similarity and 70% for Nsp14 specifically.⁴⁴ Interestingly, hCoV-229E Nsp14 knockout mutants are also not infectious.⁴⁵ SARS-CoV is closer in structural similarity to SARS-CoV-2 (80% of sequence similarity and 95% for Nsp14) but its Nsp14 mutants are still viable.¹⁰ This makes hCoV-229E a good and easy-to-handle model for a first phenotypic evaluation, whereas SARS-CoV-2 assays require specific infrastructure and equipment. We performed a dual luciferase assay in a whole-cell setting with hepatocarcinoma cell lines (Huh-7.5 FLuc) infected with hCoV-229E-luc *renilla* luciferase reporter virus and measured residual infectivity and cell viability after incubation with the compounds.⁴⁶ Compounds **4** and **8** showed dose-dependent antiviral activity with low micromolar half-maximal inhibitory concentrations (IC₅₀ = 2.3–4.6 μM), without showing any cytotoxicity (Figure 8). None of the other tested compounds showed any significant antiviral activity on hCoV-229E. Here again, we can find again the 2-(trifluoromethyl)pyridine and the 2-aminopyrimidine moieties in the two active compounds, which confirms their beneficial effect for this class, compared to the two other aldehydes. Moreover, we can notice the presence of the tetrahydrobenzothiophene in **4** along with an indole (compound **8**). The compound **1** being the less active, we can say that electron-rich aromatic rings seem beneficial compared to electron-poor ones.

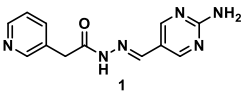
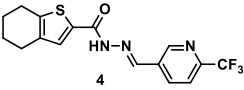


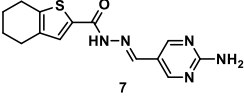
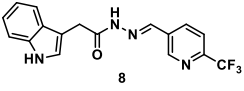
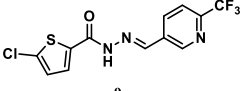
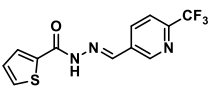
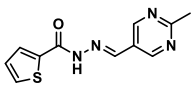
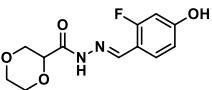
Compound	1	4	7	8
IC ₅₀ [μM]	> 10	4.62	> 10	2.33
CC ₅₀ [μM]	> 10	> 10	> 10	> 10

Figure 8 – Activity of compounds 1, 4, 7 and 8 against hCoV-229E-luc infectivity and cell viability. Huh-7.5 FLuc cells were infected with hCoV-229E-luc for 48 h in the presence of indicated compound concentrations. Renilla luciferase activity was determined as measure for residual infectivity (black circles) whereas firefly luciferase activity of the same cells represents cell viability (grey triangles). The mean and standard deviation of three biological replicates are depicted. IC₅₀ and CC₅₀ values were interpolated from regression curves.

Eight of the synthesised compounds showed interesting although different profiles (by binding Nsp10 and/or inhibiting the tested enzymatic activities) and were therefore tested for their antiviral activity against SARS-CoV-2 full-length virus in Calu-3 cells (Table 2). Compounds **4**, **7**, **8** and **14** led to a moderate decrease of the infectivity of the virus (67–88% compared to the control at 10 μM). Compounds **4** and **7** displayed promising activities in the majority of the assays, with a good binding affinity, an inhibition of the ExoN activity and of the infectivity of SARS-CoV-2 in Calu-3 cells, without showing any cytotoxicity in the whole-cell setting. Compound **4** also displays a micromolar antiviral activity against hCoV-229E. Compounds **1** and **8** bind to Nsp10, but fail to disrupt any of the enzymatic activities tested. However, compound **8** showed the best antiviral activity on both hCoV-229E and SARS-CoV-2 infectivity assay. It may have therefore another mode of action, which would need further investigation. Compounds **9**, **13** and **14** show an interesting profile, as they do not seem to bind to Nsp10 and do not display any antiviral effect on hCoV-229E, but they inhibit the ExoN or MTase activity, and compound **14** displays an antiviral activity against SARS-CoV-2. In particular, compound **9** is the most efficient of all screened compounds regarding its inhibition of ExoN activity, and was the only one that was able to disrupt the pre-formed complex. Finally, compound **11**, which does not seem to bind to Nsp10 and shows no antiviral effect on tested coronaviruses, was able to efficiently inhibit both EXoN and MTase activities. We hypothesise that these four compounds are indeed PPI inhibitors, but they may interact with some regions of the protein that are not conserved between SARS-CoV-2 and hCoV-229E. Their lack of activity in the whole-cell assay might also come from permeability issues, and calls for further optimisation of these hits.

Table 2 – Binding affinity for Nsp10, antiviral activities (hCoV-229E and SARS-CoV-2), cytotoxicity and inhibition of the ExoN and MTase activity of the most active hits obtained from tdDCC experiments 1 and 2.

Compound	K _D on Nsp10 (μM)	IC ₅₀ against the ExoN activity (μM)	IC ₅₀ against the MTase activity (μM)	IC ₅₀ against hCoV-229E (μM)	CC ₅₀ (μM)	Single dose 10 μM mean infectivity on SARS-CoV-2 [% control]
	15 ± 3	no activity	no activity	> 10	> 10	100
	90 ± 10	1505	no activity	4.6	> 10	83

	170 ± 20	1148	no activity	> 10	> 10	81
	130 ± 10	no activity	no activity	2.3	> 10	67
	no binding	343	no activity	> 10	> 10	119
	no binding	3346	577	> 10	> 10	120
	no binding	no activity	429	> 10	> 10	88
	no binding	no activity	1398	> 10	> 10	70

In general, the beneficial structural motifs are on one side the 2-trifluoromethylpyridine and the 2-aminopyrimidine moieties, and on the other side thiophene, chlorothiophene, and tetrahydrobenzothiophene. These compounds are therefore promising starting scaffolds, that open the path for further optimisation of the compounds, especially towards a better phenotypic activity.

Conclusions

In this work, we performed two tdDCC experiments to find new potential antiviral hits against SARS-CoV-2 targeting Nsp10. This non-structural protein, although not having any enzymatic function attributed, has a pleiotropic effect, since it is co-factor of both Nsp14 and Nsp16. Thus, by targeting Nsp10, we aim to inhibit the ExoN activity of Nsp14 and the MTase activity of Nsp16. Sixteen of the identified hits and controls were synthesised and evaluated for their affinity towards Nsp10 (native MS and SPR), their enzymatic activity (ExoN and MTase inhibition) and their antiviral property (infectivity on hCoV-229E and SARS-CoV-2 infected cells). The use of tdDCC successfully allowed the rapid identification of relevant hits that interact with Nsp10, and therefore are potential PPI inhibitors. However, two compounds that were not amplified and were synthesised and tested as controls were found to be active, either by binding Nsp10 like compound **8**, or by displaying an inhibition of the enzymatic activity like compound **11**. Therefore, the use of td-DCC or at least of the design of the library can be questioned for the efficient identification of Nsp10 binders. This can be because Nsp10 is not the usual protein for protein-templated synthesis, since it does not have a true pocket as a binding site, but rather a shallow surface. This could call for a different design of the protein-templated hit-finding method for this particular target.

Nevertheless, eight of the compounds displayed interesting activities, especially compounds **4** and **7**, which are active in almost all the assays, and compound **11**, which was able to inhibit both the ExoN and MTase activities of Nsp14 and Nsp16, respectively. We successfully obtained compounds that bind Nsp10 ($K_D = 15\text{--}200\ \mu\text{M}$), disturb the PPI between Nsp10 and Nsp14 or Nsp16, which result in the ExoN and MTase activity inhibition, and that are also

active in a whole-cell setting against hCoV-229E (IC_{50} = 2.3–4.6 μ M) and/or against SARS-CoV-2 (67–88% infectivity compared to the control at 10 μ M).

The most promising structural motifs are a 2-trifluoromethylpyridine or a 2-aminopyrimidine on one side, and a thiophene derivative on the other side. Although the hits obtained in this study did not show the best binding, enzymatic, and *in vivo* activity, they represent the first example of a new class of inhibitors of ExoN and MTase activity, with potential to have antiviral activity. TdDCC successfully provided hits against potential antiviral targets,⁴⁷ but to our knowledge, it is the first example of protein-templated synthesis to identify inhibitors of SARS-CoV-2. The found hits will need further optimisation in terms of activity and ADMET properties, and the validation of their mode of action should be pursued. This work indeed sets the stage for a medicinal-chemistry program to further develop the hits identified and obtain antiviral agents against SARS-CoV-2 and potential future coronaviruses.

Experimental

Detailed experimental section including materials and methods have been described in ESI.

Acknowledgements

Work at ITQB NOVA was supported by FCT - Fundação para a Ciência e a Tecnologia, I.P., through MOSTMICRO-ITQB R&D Unit (UIDB/04612/2020, UIDP/04612/2020) and LS4FUTURE Associated Laboratory (LA/P/0087/2020). It was also funded by project PTDC/BIA-BQM/28479/2017 from FCT to RGM. MS was financed by an FCT contract according to DL57/2016, [SFRH/BPD/109464/2015] and RGM by an FCT contract (ref. CEECIND/02065/2017).

T.P. received funding of the Niedersächsisches Ministerium für Wissenschaft und Kultur (Ministry for Science and Culture of Lower Saxony) (grant 14-76103-184 CORONA-13/20). T.P. received funding of the Deutsche Forschungsgemeinschaft (DFG, German Research Foundation) under Germany's Excellence Strategy – EXC 2155 “RESIST” – Project ID 390874280.

The authors acknowledge the excellent technical assistance by Anne Kühnel and Christina Grethe.

References

1. Zhu, N. *et al.* A Novel Coronavirus from Patients with Pneumonia in China, 2019. *N. Engl. J. Med.* **382**, 727–733 (2020).
2. Zhou, P. *et al.* A pneumonia outbreak associated with a new coronavirus of probable bat origin. *Nature* **579**, 270–273 (2020).
3. Singh, T. U. *et al.* Drug repurposing approach to fight COVID-19. *Pharmacol. Reports* **72**, 1479–1508 (2020).
4. Kim, D. *et al.* The Architecture of SARS-CoV-2 Transcriptome. *Cell* **181**, 914-921.e10 (2020).

5. Yadav, R. *et al.* Role of Structural and Non-Structural Proteins and Therapeutic Targets of SARS-CoV-2 for COVID-19. *Cells* **10**, 821 (2021).
6. Tahir, M. Coronavirus genomic nsp14-ExoN, structure, role, mechanism, and potential application as a drug target. *J. Med. Virol.* **93**, 4258–4264 (2021).
7. Smith, E. C., Blanc, H., Vignuzzi, M. & Denison, M. R. Coronaviruses Lacking Exoribonuclease Activity Are Susceptible to Lethal Mutagenesis: Evidence for Proofreading and Potential Therapeutics. *PLoS Pathog.* **9**, (2013).
8. Ogando, N. S. *et al.* The Enzymatic Activity of the nsp14 Exoribonuclease Is Critical for Replication of MERS-CoV and SARS-CoV-2. *J. Virol.* **94**, (2020).
9. Gribble, J. *et al.* The coronavirus proofreading exoribonuclease mediates extensive viral recombination. *PLoS Pathog.* **17**, 1–28 (2021).
10. Eckerle, L. D. *et al.* Infidelity of SARS-CoV Nsp14-exonuclease mutant virus replication is revealed by complete genome sequencing. *PLoS Pathog.* **6**, 1–15 (2010).
11. Saramago, M. *et al.* New targets for drug design: importance of nsp14/nsp10 complex formation for the 3'-5' exoribonucleolytic activity on SARS-CoV-2. *FEBS J.* **288**, 5130–5147 (2021).
12. Riccio, A. A., Sullivan, E. D. & Copeland, W. C. Activation of the SARS-CoV-2 NSP14 3'-5' exoribonuclease by NSP10 and response to antiviral inhibitors. *J. Biol. Chem.* **298**, 101518 (2022).
13. Vithani, N. *et al.* SARS-CoV-2 Nsp16 activation mechanism and a cryptic pocket with pan-coronavirus antiviral potential. *Biophys. J.* **120**, 2880–2889 (2021).
14. Alshiraihi, I. M., Klein, G. L. & Brown, M. A. Targeting NSP16 Methyltransferase for the Broad-Spectrum Clinical Management of Coronaviruses: Managing the Next Pandemic. *Diseases* **9**, 12 (2021).
15. Snijder, E. J., Decroly, E. & Ziebuhr, J. *The Nonstructural Proteins Directing Coronavirus RNA Synthesis and Processing. Advances in Virus Research* vol. 96 (Elsevier Inc., 2016).
16. Menachery, V. D., Debbink, K. & Baric, R. S. Coronavirus non-structural protein 16: Evasion, attenuation, and possible treatments. *Virus Res.* **194**, 191–199 (2014).
17. Bouvet, M. *et al.* Coronavirus Nsp10, a critical co-factor for activation of multiple replicative enzymes. *J. Biol. Chem.* **289**, 25783–25796 (2014).
18. Rogstam, A. *et al.* Crystal structure of non-structural protein 10 from severe acute respiratory syndrome coronavirus-2. *Int. J. Mol. Sci.* **21**, 1–15 (2020).
19. Lin, S. *et al.* Crystal structure of SARS-CoV-2 nsp10 bound to nsp14-ExoN domain reveals an exoribonuclease with both structural and functional integrity. *Nucleic Acids Res.* **49**, 5382–5392 (2021).
20. Rosas-Lemus, M. *et al.* High-resolution structures of the SARS-CoV-2 2'-O-methyltransferase reveal strategies for structure-based inhibitor design. *Sci. Signal.* **13**, 1–12 (2020).
21. Owen, D. R. *et al.* An oral SARS-CoV-2 Mpro inhibitor clinical candidate for the treatment of COVID-19. *Science (80-)*. **374**, 1586–1593 (2021).
22. U.S. Food and Drug Administration. Fact sheet for healthcare providers Emergency Use Authorization (EUA) for Paxlovid. *US Food Drug Adm.* 1–29 (2021).
23. Yin, W. *et al.* Structural basis for inhibition of the SARS-CoV-2 RNA polymerase by

- suramin. *Nat. Struct. Mol. Biol.* **28**, 319–325 (2021).
24. Eckerle, L. D., Lu, X., Sperry, S. M., Choi, L. & Denison, M. R. High Fidelity of Murine Hepatitis Virus Replication Is Decreased in nsp14 Exoribonuclease Mutants. *J. Virol.* **81**, 12135–12144 (2007).
 25. Graepel, K. W. *et al.* Proofreading-Deficient Coronaviruses Adapt for Increased Fitness over Long-Term Passage without Reversion of Exoribonuclease-Inactivating Mutations. *MBio* **8**, 1–16 (2017).
 26. Agostini, M. L. *et al.* Coronavirus susceptibility to the antiviral remdesivir (GS-5734) is mediated by the viral polymerase and the proofreading exoribonuclease. *MBio* **9**, (2018).
 27. Canal, B. *et al.* Identifying SARS-CoV-2 antiviral compounds by screening for small molecule inhibitors of nsp15 endoribonuclease. *Biochem. J.* **478**, 2465–2479 (2021).
 28. Kozielski, F. *et al.* Identification of fragments binding to SARS-CoV-2 nsp10 reveals ligand-binding sites in conserved interfaces between nsp10 and nsp14/nsp16. *RSC Chem. Biol.* **3**, 44–55 (2022).
 29. Rona, G. *et al.* The NSP14/NSP10 RNA repair complex as a Pan-coronavirus therapeutic target. *Cell Death Differ.* **29**, 285–292 (2022).
 30. Baddock, H. T. *et al.* Characterization of the SARS-CoV-2 ExoN (nsp14ExoN–nsp10) complex: implications for its role in viral genome stability and inhibitor identification. *Nucleic Acids Res.* **50**, 1484–1500 (2022).
 31. Bobrovs, R. *et al.* Discovery of sars-cov-2 nsp14 and nsp16 methyltransferase inhibitors by high-throughput virtual screening. *Pharmaceuticals* **14**, (2021).
 32. El Hassab, M. A. *et al.* In silico identification of novel SARS-COV-2 2'-O-methyltransferase (nsp16) inhibitors: structure-based virtual screening, molecular dynamics simulation and MM-PBSA approaches. *J. Enzyme Inhib. Med. Chem.* **36**, 727–736 (2021).
 33. Maurya, S. K., Maurya, A. K., Mishra, N. & Siddique, H. R. Virtual screening, ADME/T, and binding free energy analysis of anti-viral, anti-protease, and anti-infectious compounds against NSP10/NSP16 methyltransferase and main protease of SARS CoV-2. *J. Recept. Signal Transduct.* **40**, 605–612 (2020).
 34. Hartman, A. M., Gierse, R. M. & Hirsch, A. K. H. Protein-Templated Dynamic Combinatorial Chemistry: Brief Overview and Experimental Protocol. *European J. Org. Chem.* **2019**, 3581–3590 (2019).
 35. Mondal, M. & Hirsch, A. K. H. Dynamic combinatorial chemistry: A tool to facilitate the identification of inhibitors for protein targets. *Chem. Soc. Rev.* **44**, 2455–2488 (2015).
 36. Jumde, R. P. *et al.* Hit-optimization using target-directed dynamic combinatorial chemistry: development of inhibitors of the anti-infective target 1-deoxy- β -D-xylulose-5-phosphate synthase. *Chem. Sci.* **12**, 7775–7785 (2021).
 37. Bhat, V. T. *et al.* Nucleophilic catalysis of acylhydrazone equilibration for protein-directed dynamic covalent chemistry. *Nat. Chem.* **2**, 490–497 (2010).
 38. Demetriades, M. *et al.* Dynamic Combinatorial Chemistry Employing Boronic Acids/Boronate Esters Leads to Potent Oxygenase Inhibitors. *Angew. Chemie Int. Ed.* **51**, 6672–6675 (2012).
 39. Hartman, A. M. *et al.* Discovery of Small-Molecule Stabilizers of 14-3-3 Protein-Protein Interactions via Dynamic Combinatorial Chemistry. *ACS Med. Chem. Lett.* **11**, 1041–1046 (2020).

40. Bamford, W. R. & Stevens, T. S. 924. The decomposition of toluene-p-sulphonylhydrazones by alkali. *J. Chem. Soc.* **5**, 4735 (1952).
41. Gavriilidou, A. F. M., Sokratous, K., Yen, H.-Y. & De Colibus, L. High-Throughput Native Mass Spectrometry Screening in Drug Discovery. *Front. Mol. Biosci.* **9**, 1–15 (2022).
42. Lin, S. *et al.* Crystal structure of SARS-CoV-2 nsp10 bound to nsp14-ExoN domain reveals an exoribonuclease with both structural and functional integrity. *Nucleic Acids Res.* **49**, 5382–5392 (2021).
43. Pene, F. *et al.* Coronavirus 229E-Related Pneumonia in Immunocompromised Patients. *Clin. Infect. Dis.* **37**, 929–932 (2003).
44. Hsu, J. C. C., Laurent-Rolle, M., Pawlak, J. B., Wilen, C. B. & Cresswell, P. Translational shutdown and evasion of the innate immune response by SARS-CoV-2 NSP14 protein. *Proc. Natl. Acad. Sci. U. S. A.* **118**, 1–9 (2021).
45. Minskaia, E. *et al.* Discovery of an RNA virus 3'→5' exoribonuclease that is critically involved in coronavirus RNA synthesis. *Proc. Natl. Acad. Sci.* **103**, 5108–5113 (2006).
46. van den Worm, S. H. E. *et al.* Reverse Genetics of SARS-Related Coronavirus Using Vaccinia Virus-Based Recombination. *PLoS One* **7**, e32857 (2012).
47. Mondal, M. *et al.* Fragment Linking and Optimization of Inhibitors of the Aspartic Protease Endothiapepsin: Fragment-Based Drug Design Facilitated by Dynamic Combinatorial Chemistry. *Angew. Chemie - Int. Ed.* **55**, 9422–9426 (2016).